



Sustained Kozai–Lidov Oscillations in Misaligned Circumstellar Gas Disks

Jeremy L. Smallwood¹, Rebecca G. Martin¹, and Stephen H. Lubow²¹ Department of Physics and Astronomy, University of Nevada, Las Vegas, 4505 South Maryland Parkway, Las Vegas, NV 89154, USA; smallj2@unlv.nevada.edu² Space Telescope Science Institute, Baltimore, MD 21218, USA

Received 2020 October 13; revised 2020 December 16; accepted 2020 December 18; published 2021 January 19

Abstract

A disk around one component of a binary star system with sufficiently high inclination can undergo Kozai–Lidov (KL) oscillations during which the disk inclination and disk eccentricity are exchanged. Previous studies show that without a source of accretion, KL unstable disks exhibit damped oscillations, due to viscous dissipation, that leave the disk stable near or below the critical inclination for KL oscillations. With three-dimensional hydrodynamical simulations we show that a highly misaligned circumbinary disk that flows onto the binary components forms highly inclined circumstellar disks around each component. We show that a continuous infall of highly inclined material allows the KL oscillations to continue. The KL disk oscillations produce shocks and eccentricity growth in the circumstellar disks that affect the conditions for planet formation.

Unified Astronomy Thesaurus concepts: [Binary stars \(154\)](#); [Stellar accretion disks \(1579\)](#); [Exoplanet formation \(492\)](#)

1. Introduction

Circumbinary gas disks have a central cavity caused by the tidal torque produced by Lindblad resonances due to the central binary (Artymowicz & Lubow 1994; Lubow et al. 2015; Miranda & Lai 2015). The cavity size is determined by the radius where tidal torques balance viscous torques. This balance between viscous and tidal torques is determined in a one-dimensional azimuthally averaged sense and neglects nonaxisymmetric imbalances that could arise in multiple dimensions. The central binary produces an outward torque that, in the simplest models, prevents circumbinary material from flowing onto the central binary (Lynden-Bell & Pringle 1974; Pringle 1991).

In spite of this central cavity and outward torque, material can flow through the cavity as gas streams (Artymowicz & Lubow 1996; Günther & Kley 2002; Shi et al. 2012; D’Orazio et al. 2013; Farris et al. 2014; Muñoz et al. 2019). This flow forms and/or replenishes circumstellar disks of gas and dust around each component of a binary. For typically warm and viscous protostellar disks, the accretion rate onto the central binary is comparable to the rate that would occur if the the binary were replaced by a single star, even though viscous and tidal torques are balanced in the one-dimensional (radial) sense at the inner edge of the circumbinary disk. Based on simulations at a few different disk aspect ratios H/R , Artymowicz & Lubow (1996) originally suggested that $H/R \gtrsim 0.05$, if the turbulent viscosity parameter α is greater than 0.01, is required for efficient (unimpeded) flow into the cavity. Using more accurate simulations and more H/R values, Ragusa et al. (2016) suggested that $H/R \gtrsim 0.1$ is required for efficient flow.

Circumbinary disks are sometimes observed to be misaligned to the binary orbital plane, particularly during early stages of stellar evolution. The pre-main-sequence binary KH 15D has a low inclination ($\sim 3\text{--}15^\circ$) precessing circumbinary ring or disk (Chiang & Murray-Clay 2004; Lodato & Facchini 2013; Smallwood et al. 2019; Poon et al. 2020). The circumbinary disk around the young binary IRS 43 has an observed misalignment of $\sim 60^\circ$ (Brinch et al. 2016). There is

an observed misalignment of $\sim 70^\circ$ between the circumbinary disk and the circumprimary disk in HD 142527 (Marino et al. 2015; Owen & Lai 2017). The 6–10 Gyr old binary system, 99 Herculis, has a nearly polar ($\sim 87^\circ$) debris ring (Kennedy et al. 2012; Smallwood et al. 2020). The gaseous circumbinary disk around HD 98800BaBb is found to be nearly polar (Kennedy et al. 2019). There is evidence that the circumbinary disk around GG Tau is misaligned by $\sim 30^\circ$ (Aly et al. 2018).

Kozai–Lidov (KL) oscillations were first studied for test particles that reside in orbits that are highly misaligned to the orbital plane of a circular orbit binary (Kozai 1962; Lidov 1962). The particle orbits undergo oscillations in which eccentricity and inclination are exchanged. An initially highly inclined circular orbit can periodically obtain high eccentricity during phases of lower inclination. For eccentric orbit binaries, stronger effects from KL oscillations have been found to occur (Lithwick & Naoz 2011; Teyssandier et al. 2013; Liu et al. 2015). Tidal dissipational effects on KL planets were analyzed by Fabrycky & Tremaine (2007).

A misaligned circumbinary disk may form misaligned circumstellar disks around each binary component (e.g., Nixon et al. 2013). If a circumstellar disk around a binary component is sufficiently misaligned with respect to the binary orbital plane and has a sufficiently low disk aspect ratio, the disk may also undergo KL oscillations in which the disk eccentricity and inclination are exchanged (Martin et al. 2014a). Simulations suggest that the critical inclination above which KL oscillations occurs is approximately equal to the value for particles of 40° , although linear theory suggests that it varies with the disk aspect ratio (Lubow & Ogilvie 2017; Zanazzi & Lai 2017). Linear theory also suggests that $H/R \lesssim 0.15$ is typically required for an equal-mass binary.

The properties of KL oscillations of particles and disks differ. KL oscillations of a set of particle orbits have a tilt frequency that varies with distance from the central star, resulting in an incoherent overall tilt. A gaseous disk however can undergo a coherent tilt oscillation whose frequency is independent of radius due to the effects of pressure forces. In addition, the KL disk oscillations damp over time due to dissipation, which does not occur for test particles.

In this Letter, we investigate the evolution of a highly misaligned KL unstable circumstellar disk that forms through accretion from a misaligned circumbinary disk. Previous models of disks undergoing the KL mechanism found that the KL cycles damp due to viscous dissipation. The lack of accretion of misaligned material onto the circumstellar disks in these models caused their inclinations to evolve to near or below the KL critical angle for test particles (about 39°) and the cycles ended (Martin et al. 2014a; Fu et al. 2015a, 2015b; Franchini et al. 2019).

However, since our simulation includes a misaligned circumbinary disk, the KL unstable circumstellar disks have a reservoir of misaligned material that continues to flow through the binary cavity and accrete onto the circumstellar disks. As a result, we find that the KL mechanism can be long-lived. This has implications for the accretion variability in time. The mechanism also has implications for planet formation within binary star systems. A circumstellar disk undergoing KL oscillations experiences periodic changes in eccentricity that affect the interaction of the gas with the solids. In this Letter, we focus only on the properties of the gas. The disk can experience strong shocks during high-eccentricity phases that can affect the conditions for planet formation. In particular, such a disk may undergo gravitational instability and fragmentation (Fu et al. 2017).

The outline of this Letter is as follows. In Section 2, we describe the setup and results of our hydrodynamical disk simulation. We discuss the relevance and implications of this work in Section 3. Finally, we give concluding remarks in Section 4.

2. Hydrodynamical Disk Simulations

We model the evolution of an initially flat but misaligned hydrodynamical circumbinary disk with PHANTOM (Price et al. 2018). The PHANTOM code is a three-dimensional smoothed particle hydrodynamics (SPH) code that has been tested extensively for modeling misaligned accretion disks (e.g., Nixon et al. 2012, 2013; Doğan et al. 2015; Nixon & Lubow 2015; Facchini et al. 2018; Smallwood et al. 2019; Aly & Lodato 2020).

2.1. Setup

In this section, we describe the setup of the hydrodynamical simulations. We consider an equal-mass binary with an eccentricity of $e_b = 0.1$. The binary begins at apastron at $t = 0$. We apply a mass sink about each star that has an accretion radius. When a particle penetrates the accretion radius, it is accreted onto the sink and the particle's mass and angular momentum are added to the star (e.g., Bate et al. 1995). Larger accretion radii eliminate the need to resolve particle orbits close to the stars, which speeds up computational time significantly. However, since we want to resolve the formation of circumstellar material, the accretion radius for each star is chosen to be $0.05a$, where a is the binary semimajor axis. The accretion radius is a hard boundary, meaning that all of the particles that enter are accreted and their mass and angular momentum are added to the sink particle.

The circumbinary disk is initially misaligned by 60° to the binary orbital plane that is initially in the x - y plane. The binary begins at apastron and along the x -axis. The disk is initially comprised of 1.5×10^6 equal-mass Lagrangian particles. The

simulation end time is set to $45 P_{\text{orb}}$, which is sufficient to reach a quasi-steady state, where P_{orb} is the binary orbital period. We simulate a low-mass circumbinary disk such that $M_{\text{CBD}} = 10^{-3}M$, where M is the binary mass. The particles are initially located in a flat circumbinary disk with an inner disk radius of $R_{\text{in}} = 1.6a$ and an outer disk radius of $R_{\text{out}} = 2.6a$. The inner boundary of the disk is chosen to be smaller than where the binary tidal torque truncates the inner edge of an aligned disk (Artymowicz & Lubow 1994). The tidal torque for a misaligned disk is weaker which allows the inner disk radius to be closer to the binary (e.g., Lubow et al. 2015; Miranda & Lai 2015).

The physical disk viscosity is modeled using the artificial viscosity α^{av} , which is implemented in PHANTOM (Lodato & Price 2010). The circumbinary disk has an initial surface density profile of the form $\Sigma \propto R^{-3/2}$, and the disk aspect ratio H/R is set to be 0.1 at R_{in} . With this prescription, the shell-averaged smoothing length per scale height $\langle h \rangle/H$ and the disk viscosity parameter α are constant over the radial extent of the disk (Lodato & Pringle 2007). We take a relatively high Shakura & Sunyaev (1973) α_{SS} parameter of 0.1 in order to increase the resolution of the circumstellar disks by having a relatively high inflow rate from the circumbinary disk into the binary cavity. The circumbinary disk is initially resolved with $\langle h \rangle/H = 0.11$.

Traditionally, to model the evolution of a circumbinary disk, it is efficient to use a locally isothermal temperature profile centered on the binary center of mass. This model does not accurately apply to circumstellar disks. Since we are interested in forming circumstellar disks from the inflow of circumbinary gas, we adopt the locally isothermal equation of state of Farris et al. (2014) and set the sound speed c_s to be

$$c_s = \mathcal{F} c_{s0} \left(\frac{a}{M_1 + M_2} \right)^q \left(\frac{M_1}{R_1} + \frac{M_2}{R_2} \right)^q, \quad (1)$$

where R_1 and R_2 are the radial distances from the primary and secondary stars, respectively, and c_{s0} is a constant with dimensions of velocity. Parameter q is set to $3/4$. \mathcal{F} is a dimensionless function of position that we define below. The binary total mass is $M = M_1 + M_2$, where M_1 and M_2 are the masses of the primary and secondary stars, respectively. This prescription of the sound speed ensures that the temperatures in the circumprimary and circumsecondary disks are mainly set by the primary and secondary stars, respectively. For $R_1, R_2 \gg a$, the sound speed is set by the distance from the binary center of mass.

To further improve the resolution of the circumstellar disks, we introduce function \mathcal{F} in Equation (1) to decrease the sound speed close to each binary component, thus leading to a longer viscous timescale and more mass in the steady-state disk. We take

$$\mathcal{F} = \begin{cases} \sqrt{0.001}, & \text{if } R_1 \text{ or } R_2 < R_c, \\ 1, & \text{otherwise,} \end{cases} \quad (2)$$

where R_c is the cutoff radius. We ran extensive tests to determine the optimal value of R_c . If this value is too small (close to the binary), disk formation will be suppressed, due to the low resolution caused by the larger separation between the particles. On the other hand, a cutoff radius that is too far from the binary components will affect the circumbinary disk. We

adopt a cutoff radius of $R_c = 0.35a$ from each binary component.

Beyond this cutoff distance from a binary component, the gas flow through the gap has not encountered the bound material orbiting that binary component. Consequently, there are no shocks beyond the cutoff radius involving that component’s circumstellar disk. With this prescription, the disk aspect ratio of the circumstellar disks at radius $r = 0.1a$ is $H/R \sim 0.01$. This aspect ratio is one-tenth of the disk aspect ratio at the initial inner circumbinary disk radius. Since the motion of the gas streams that flow through the gap is supersonic, the gas temperature has little effect on that flow. The properties of the gas flow that transports material from the circumbinary disk toward the circumstellar disks should then be similar with and without this factor. The factor \mathcal{F} results in a stronger shock when the inflowing gas encounters a circumstellar disk that in turn results in a higher post-shock density and hence higher resolution. This factor also significantly increases the resolution within the forming circumstellar disk, however, the resolution is not as high as that of the circumbinary disk. We have tried numerous additional approaches to increase the resolution of the circumstellar disks while also still resolving the circumbinary disk but to no avail. The current approach presented in this Letter is the best option we have found for the smoothed particle hydrodynamics simulations we present.

2.2. Results

In this section, we explore the formation of circumstellar disks from material initially originating from a highly misaligned circumbinary disk. We extract the disk parameters as a function of time. To analyze the data on the circumbinary disk, we average over all particles which range from the innermost bound circumbinary particle out to a distance of $3a$. For the circumstellar disks, we average over all particles that are bound to each binary component (i.e., the specific energies, kinetic plus potential, of the particles are negative, neglecting the thermal energy). For each disk, we calculate the mean properties of the particles such as the surface density, inclination, longitude of ascending node, and eccentricity.

Figure 1 shows the formation of circumstellar disks from the highly misaligned circumbinary disk at a time of $t = 18 P_{\text{orb}}$. Both the circumprimary and circumsecondary disks are becoming moderately eccentric due to the KL mechanism. Figure 2 shows the inclination, eccentricity, longitude of the ascending node, disk mass, and accretion rate as a function of time in units of the binary orbital period. We plot the properties of only the circumprimary and circumbinary disks. We note that the circumsecondary disk has similar disk properties to the circumprimary disk. Panel 1 shows the disk inclination evolution. The circumprimary disk initially forms with an inclination of $\sim 80^\circ$. Note that the initial misalignment of the circumbinary disk is 60° and remains at a similar inclination throughout the simulation. Therefore, the circumstellar disks form at a higher inclination than the initial circumbinary disk inclination. The circumprimary and circumsecondary disks undergo KL cycles, since the inclinations are above the critical angle for test particles of about 39° . For a gas disk, the criteria to induce KL cycles also depends on the disk aspect ratio (Lubow & Ogilvie 2017; Zanazzi & Lai 2017). If the aspect ratio H/R is too high, greater than roughly 0.15 for an equal-mass binary, the KL oscillations can be suppressed.

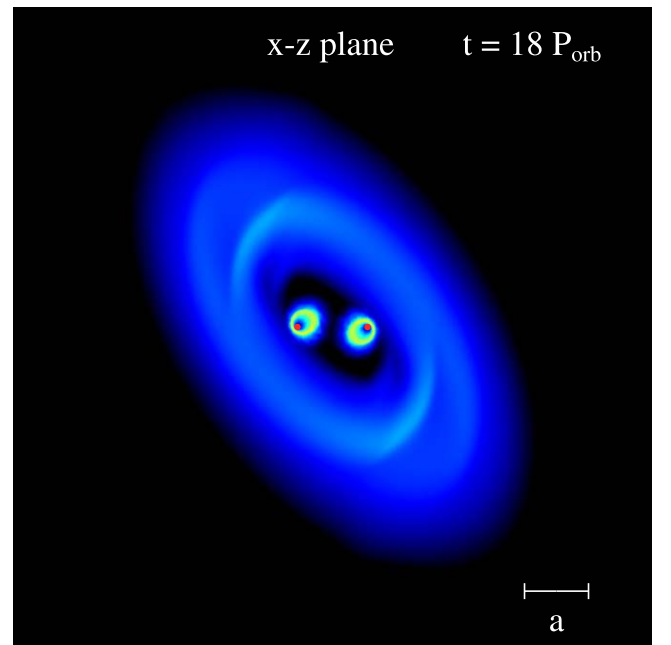


Figure 1. The formation of circumstellar disks from a low-mass circumbinary disk that is initially inclined by 60° at $t = 18 P_{\text{orb}}$. The eccentric orbit binary components are denoted by the red circles. The color denotes the gas density using a density-weighted interpolation, which gives a mass-weighted line-of-sight average. The yellow regions are about three orders of magnitude larger than the blue. At this time, the circumstellar disks are gaining eccentricity due to the KL mechanism. The view is in the x - z plane.

Panel 2 shows the disk eccentricity as a function of time. After $\sim 2 P_{\text{orb}}$, the material that falls in has eccentricity around 0.2, before any KL oscillations are established. At later times there are repeated oscillations of eccentricity growth. The maximum eccentricity induced is ~ 0.63 . Comparing the top two panels in Figure 2, we see that as the eccentricity increases the inclination decreases, and vice versa, which is indicative of the KL mechanism operating. The period of the KL oscillations is about $6 P_{\text{orb}}$, which is similar to the period found in previous work on KL disks (Martin et al. 2014b). The KL cycles that are induced do not quickly damp as previous models have found due to the fact the circumstellar disks are continuously fed by high-inclination material originating from the circumbinary disk. However, the amplitude of the oscillations decrease somewhat with time, which is due to the depletion of mass in the circumbinary disk. At $45 P_{\text{orb}}$, the circumbinary disk has lost $\sim 40\%$ of its initial mass. Moreover, the minimum eccentricity during the KL oscillations is larger than the eccentricity of the infalling material of ~ 0.2 . This means that the KL unstable disks are able to maintain a disk structure, rather than becoming completely accreted during each high-eccentricity phase and then recreated.

Panel 3 in Figure 2 shows the longitude of the ascending node as a function of time. The circumstellar disk begins to precess as it is formed and it precesses at a faster rate than the circumbinary disk. Panel 4 shows the evolution of the circumprimary disk mass. Due to the large disk aspect ratio and high viscosity, there is a high infall rate of material into the cavity within the first $5 P_{\text{orb}}$. This causes the circumstellar disk mass to grow rapidly. However, beyond $5 P_{\text{orb}}$, the mass in both circumstellar disks reach a quasi-steady state. The accretion rate peaks at times when the eccentricity is locally maximum. At the times of each maximum (minimum) in

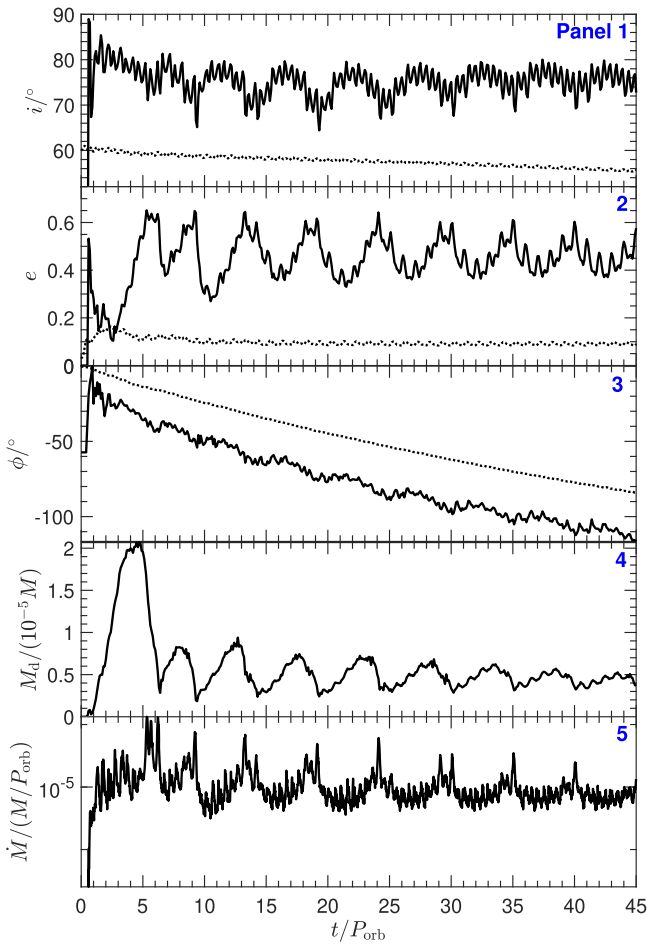


Figure 2. Disk parameters for the circumprimary disk (solid) and circumbinary disk (dotted) as a function of time in units of the binary orbital period. The disk parameters are inclination i (Panel 1), eccentricity e (2), longitude of the ascending node ϕ (3), disk mass M_{disk} (4), and mass accretion rate \dot{M} (5). The circumbinary disk results are only shown for the top three panels.

eccentricity, the disk’s mass decreases (increases) due to the increased (decreased) accretion rate onto the binary components. Panel 5 shows the accretion rate on a log scale as a function of time.

Lastly, we examine the evolution of the surface density of the circumprimary disk. Since we are modeling an equal-mass binary, the evolution of the circumprimary and circumsecondary disks are similar. Figure 3 shows the circumprimary disk surface density at times $t = 18 P_{\text{orb}}$ and $20 P_{\text{orb}}$. The disk forms at a time $\sim 2 P_{\text{orb}}$. At $t = 18 P_{\text{orb}}$, there is a locally maximum disk mass and an increasing eccentricity. At a time $t = 20 P_{\text{orb}}$, there is a locally minimum disk mass and decreasing eccentricity. Since we have found that the KL cycles are continuous, the surface density of the circumstellar disks continuously oscillates between the black and blue lines.

3. Discussion

Binary stars are common within the Galaxy (e.g., Duquennoy & Mayor 1991; Raghavan et al. 2010). It has been estimated that roughly 50% of the discovered exoplanets may be hosted by binary systems (Horch et al. 2014; Deacon et al. 2016; Ziegler et al. 2018). For example, the binary system γ Cep AB has a separation of ~ 20 au and hosts a giant planet around the primary star, γ Cep Ab (Hatzes et al. 2003). The

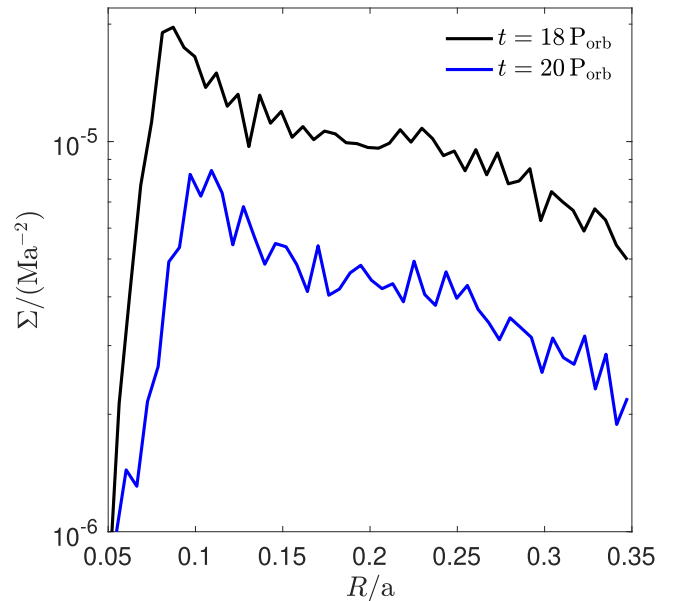


Figure 3. The surface density profile as a function of radius for an inclined circumprimary disk. The surface density profile is shown at two different times: $18 P_{\text{orb}}$ (black) and $20 P_{\text{orb}}$ (blue).

planet formation process is thought to take place in a protoplanetary disk. For the cases of binary star systems, material from a circumbinary disk can feed the circumstellar disks in which planets may form. The effects of KL oscillations of the circumstellar disks found in this Letter play an important role in affecting the formation of planets around each individual binary component involving a misaligned circum-binary disk.

The KL mechanism operates in binary systems in cases in which the circumstellar disks are highly misaligned to the binary orbital plane. Fu et al. (2017) found that strong shocks are generated in the circumstellar disks when the eccentricity is high. Their models had KL cycles that damped due to viscous dissipation. Since we have shown that KL cycles can be sustained for longer periods of time, shocks will be generated on each KL cycle, which will impact the formation of S-type planets in binaries. In sufficiently massive disks shocks may trigger the gravitational instability (GI), which is a possible theory to form giant planets (Boss 1997). Therefore, the KL mechanism can cause disk GI, which leads to fragmentation and efficient formation of giant planets (Fu et al. 2017).

Massive circumbinary disks will provide both an accretional torque and gravitational torque on the binary, which will affect the binary orbital evolution (Muñoz et al. 2019), and thus affect the misalignment evolution (Martin & Lubow 2019). For an initially low-eccentricity binary, $e_b = 0.1$ (which is used in our hydrodynamical simulations), Artymowicz et al. (1991) found that the binary eccentricity is increasing due to gravitational effects of the disk. For fixed binary semimajor axis, circumstellar disk radii decrease with increasing binary eccentricity (Artymowicz & Lubow 1994; Miranda & Lai 2015).

The presence of a circumbinary disk allows for a reservoir of material that accretes onto the forming circumstellar disks. Throughout the simulation, the misalignment of the circumbinary disk remains nearly constant. However, the resulting circumstellar disks form initially at a higher inclination and then proceed to undergo the KL mechanism where the

inclination oscillates. The KL cycles are more periodic when including the accretion of material from the circumbinary disk. However, the cycles do not repeat as precisely as in the case of test particle orbits. This is a result of the KL mechanism being sensitive to the binary and disk parameters that are changing in time (e.g., Fu et al. 2015a). For example, the circumbinary disk depletes to about 40% the initial disk mass at the end of the simulation. During this process, material is continuously being transported with high inclination to the lower inclination circumstellar disk. Accretion keeps the inclination of the disk high and allows the KL cycles to continue. However, if circumstellar disk material were to accrete on a timescale shorter than the KL oscillation period, we would not expect the KL oscillations to operate. In this work, we consider an equal-mass binary. However, for an unequal mass binary, we expect that the KL oscillations would be qualitatively similar. But the gas stream feeding will not be the same for the two circumstellar disks and their oscillation properties will differ.

Previous studies have suggested that tidally induced shocks could play an important role in causing disk accretion (e.g., Goodman & Rafikov 2001; Ju et al. 2017). From Panel 5 in Figure 2 and also Figure 3, we see that there are KL induced variations of the mass accretion rate and disk density that are likely attributable to accretion by shocks. Some of the accretion may also be due to higher eccentricity material entering the mass sink.

4. Conclusions

In this Letter, we have shown that the KL mechanism can be repeatedly sustained without damping when the circumstellar disks are replenished from a highly misaligned circumbinary disk. For example, a circumbinary disk with an initial misalignment of 60° to the binary orbital plane forms circumstellar disks that are initially inclined by $\sim 80^\circ$. Since the inclinations of the newly formed disks are larger than the KL critical angle and the disk aspect ratio criterion is met, the disks undergo KL oscillations, where the inclination is exchanged for eccentricity and vice versa. Previous models of the KL disks are damped due to viscous dissipation in the absence of accretion from a circumbinary disk. By modeling the formation of circumstellar disks from the circumbinary disk, the KL cycles are long-lived due to a large reservoir of noncoplanar material infalling from the circumbinary disk and continuously accreting onto the circumstellar disks. The longevity of the KL mechanism has important implications for planet formation in binary star systems.

We thank Daniel Price for providing the PHANTOM code for SPH simulations and acknowledge the use of SPLASH (Price 2007) for the rendering of the figures. Computer support was provided by UNLV's National Supercomputing Center. We acknowledge support from NASA XRP grant 80NSSC19K0443.

ORCID iDs

Jeremy L. Smallwood  <https://orcid.org/0000-0002-4314-398X>

Rebecca G. Martin  <https://orcid.org/0000-0003-2401-7168>
Stephen H. Lubow  <https://orcid.org/0000-0002-4636-7348>

References

- Aly, H., & Lodato, G. 2020, *MNRAS*, 492, 3306
Aly, H., Lodato, G., & Cazzoletti, P. 2018, *MNRAS*, 480, 4738
Artymowicz, P., Clarke, C. J., Lubow, S. H., & Pringle, J. E. 1991, *ApJL*, 370, L35
Artymowicz, P., & Lubow, S. H. 1994, *ApJ*, 421, 651
Artymowicz, P., & Lubow, S. H. 1996, *ApJL*, 467, L77
Bate, M. R., Bonnell, I. A., & Price, N. M. 1995, *MNRAS*, 277, 362
Boss, A. P. 1997, *Sci*, 276, 1836
Brinch, C., Jørgensen, J. K., Hogerheijde, M. R., Nelson, R. P., & Gressel, O. 2016, *ApJL*, 830, L16
Chiang, E. I., & Murray-Clay, R. A. 2004, *ApJ*, 607, 913
Deacon, N. R., Kraus, A. L., Mann, A. W., et al. 2016, *MNRAS*, 455, 4212
D'Orazio, D. J., Haiman, Z., & MacFadyen, A. 2013, *MNRAS*, 436, 2997
Doğan, S., Nixon, C., King, A., & Price, D. J. 2015, *MNRAS*, 449, 1251
Duquennoy, A., & Mayor, M. 1991, *A&A*, 248, 485
Fabrycky, D., & Tremaine, S. 2007, *ApJ*, 669, 1298
Facchini, S., Juhász, A., & Lodato, G. 2018, *MNRAS*, 473, 4459
Farris, B. D., Duffell, P., MacFadyen, A. I., & Haiman, Z. 2014, *ApJ*, 783, 134
Franchini, A., Martin, R. G., & Lubow, S. H. 2019, *MNRAS*, 485, 315
Fu, W., Lubow, S. H., & Martin, R. G. 2015a, *ApJ*, 807, 75
Fu, W., Lubow, S. H., & Martin, R. G. 2015b, *ApJ*, 813, 105
Fu, W., Lubow, S. H., & Martin, R. G. 2017, *ApJL*, 835, L29
Goodman, J., & Rafikov, R. R. 2001, *ApJ*, 552, 793
Günther, R., & Kley, W. 2002, *A&A*, 387, 550
Hatzes, A. P., Cochran, W. D., Endl, M., et al. 2003, *ApJ*, 599, 1383
Horch, E. P., Howell, S. B., Everett, M. E., & Ciardi, D. R. 2014, *ApJ*, 795, 60
Ju, W., Stone, J. M., & Zhu, Z. 2017, *ApJ*, 841, 29
Kennedy, G. M., Matrà, L., Facchini, S., et al. 2019, *NatAs*, 3, 230
Kennedy, G. M., Wyatt, M. C., Sibthorpe, B., et al. 2012, *MNRAS*, 421, 2264
Kozai, Y. 1962, *AJ*, 67, 591
Lidov, M. L. 1962, *P&SS*, 9, 719
Lithwick, Y., & Naoz, S. 2011, *ApJ*, 742, 94
Liu, B., Muñoz, D. J., & Lai, D. 2015, *MNRAS*, 447, 747
Lodato, G., & Facchini, S. 2013, *MNRAS*, 433, 2157
Lodato, G., & Price, D. J. 2010, *MNRAS*, 405, 1212
Lodato, G., & Pringle, J. E. 2007, *MNRAS*, 381, 1287
Lubow, S. H., Martin, R. G., & Nixon, C. 2015, *ApJ*, 800, 96
Lubow, S. H., & Ogilvie, G. I. 2017, *MNRAS*, 469, 4292
Lynden-Bell, D., & Pringle, J. E. 1974, *MNRAS*, 168, 603
Marino, S., Perez, S., & Casassus, S. 2015, *ApJL*, 798, L44
Martin, R. G., & Lubow, S. H. 2019, *MNRAS*, 490, 1332
Martin, R. G., Nixon, C., Armitage, P. J., Lubow, S. H., & Price, D. J. 2014a, *ApJL*, 790, L34
Martin, R. G., Nixon, C., Lubow, S. H., et al. 2014b, *ApJL*, 792, L33
Miranda, R., & Lai, D. 2015, *MNRAS*, 452, 2396
Muñoz, D. J., Miranda, R., & Lai, D. 2019, *ApJ*, 871, 84
Nixon, C., King, A., & Price, D. 2013, *MNRAS*, 434, 1946
Nixon, C., & Lubow, S. H. 2015, *MNRAS*, 448, 3472
Nixon, C. J., King, A. R., & Price, D. J. 2012, *MNRAS*, 422, 2547
Owen, J. E., & Lai, D. 2017, *MNRAS*, 469, 2834
Poon, M., Zanazzi, J. J., & Zhu, W. 2020, arXiv:2009.14204
Price, D. J. 2007, *PASA*, 24, 159
Price, D. J., Wurster, J., Tricco, T. S., et al. 2018, *PASA*, 35, e031
Pringle, J. E. 1991, *MNRAS*, 248, 754
Raghavan, D., McAlister, H. A., Henry, T. J., et al. 2010, *ApJS*, 190, 1
Ragusa, E., Lodato, G., & Price, D. J. 2016, *MNRAS*, 460, 1243
Shakura, N. I., & Sunyaev, R. A. 1973, *A&A*, 24, 337
Shi, J.-M., Krolik, J. H., Lubow, S. H., & Hawley, J. F. 2012, *ApJ*, 749, 118
Smallwood, J. L., Franchini, A., Chen, C., et al. 2020, *MNRAS*, 494, 487
Smallwood, J. L., Lubow, S. H., Franchini, A., & Martin, R. G. 2019, *MNRAS*, 486, 2919
Teyssandier, J., Terquem, C., & Papaloizou, J. C. B. 2013, *MNRAS*, 428, 658
Zanazzi, J. J., & Lai, D. 2017, *MNRAS*, 467, 1957
Ziegler, C., Law, N. M., Baranec, C., et al. 2018, *AJ*, 155, 161